Arabian Journal of Geosciences (2019) 12: 374
https://doi.org/10.1007/s12517-019-4535-5

ORIGINAL PAPER

The latest tectonic magmatism in the Buqingshan–A'nyemaqen tectonic mélange belt: evidence from zircon U–Pb geochronology of intermediate–basic dikes, northern Tibetan Plateau, China

Zuochen Li[1,2] · Xianzhi Pei[1] · Ruibao Li[1] · Lei Pei[1] · Youxin Chen[1] · Chengjun Liu[1] · Zhanqing Liu[3] · Guochao Chen[4] · Meng Wang[1] · Shaowei Zhao[1]

Received: 7 November 2018 / Accepted: 16 May 2019 / Published online: 5 June 2019

Abstract

This study focuses on the zircon U–Pb geochronology and geochemistry of intermediate–basic dikes from the Buqingshan–A'nyemaqen tectonic mélange belt (BTMB) along the southern margin of the East Kunlun orogenic belt (EKOB). Zircons from a diorite dike show oscillatory zoning and relatively high Th/U ratios (0.47–2.43), indicating that they are of magmatic origin. Using LA–ICP–MS, zircons of the diorite dike yield a U–Pb age of 205 ± 1 Ma (MSWD = 0.88), implying that the diorite dikes were formed in the Late Triassic (Rhaetian) and also represented the latest tectonic magmatism in the BTMB. Geochemical analyses show that the rocks have low SiO_2 (51.96–59.33 wt%), low Al_2O_3 (10.49–13.95 wt%), and low alkaline (4.00–5.29 wt.%), and thus belong to the subalkaline magma series. The contents of rare earth elements (REEs) are 80.23–189.19 ppm, with weakly negative to weakly positive Eu anomalies (δEu = 0.50–1.10). The trace element geochemistry is characterized by negative anomalies of Nb, Hf, P, Ti, and Sr and by positive anomalies of Th, La, Nd, Sm, Zr, and Eu. The diorite dikes, the product of a mafic magma formed at high temperature (~ 777 °C), were derived by partial melting of the mantle with possible admixture of crustal material. The intermediate–basic dikes in the BTMB are the products of mantle enriched upward and emplaced along tensional faults in the crustal–relaxation stage after the subduction–collision of the Bayan Har and East Kunlun Blocks during the Late Hercynian–Early Triassic.

Keywords Intermediate–basic dikes · Zircon U–Pb age · Geochemistry · Tectonic setting · Buqingshan–A'nyemaqen tectonic mélange belt

Editorial handling: J. S. Armstrong-Altrin

✉ Xianzhi Pei
peixzh@163.com

Zuochen Li
lizuochen2003@163.com; zuochen.li@mnf.uni-tuebingen.de

[1] Key Laboratory of Western China's Mineral Resources and Geological Engineering, Ministry of Education, Key Laboratory for the Study of Focused Magmatism and Giant Ore Deposits, Ministry of Natural Resources, Faculty of Earth Science and Resources, Chang'an University, Xi'an 710054, China

[2] Department of Geosciences, Eberhard Karls University Tübingen, 72074 Tübingen, Germany

[3] College of Earth Sciences, Guilin University of Technology, Guilin 541004, China

[4] School of Civil Engineering, Nanyang Institute of Technology, Nanyang 473000, China

Introduction

The Buqingshan–A'nyemaqen tectonic mélange belt (BTMB) is in the western part of the A'nyemaqen Suture Zone, which is at the intersection of the East Kunlun, West Qinling, and Songpan–Bayan Har orogenic belts (Fig. 1a). The mélange belt forms a junction with the Qinghai–Tibetan Plateau in the Qinling orogen and is an important tectonic component of the complex eastern section of the Proto-Tethyan and Paleo-Tethyan ocean systems (Bian and Zheng 1992; Jiang et al. 1992; Xu et al. 1996, 2001, 2006a, 2013; Wang et al. 1997a; Pei 2001; Zhang et al. 2003; Pei et al. 2018). The region experienced two main tectonic phases: the Hercynian and the Indosinian. This multi-stage history of the region is vital to understand the tectonic evolution of continental China (Jiang et al. 1992; Xu et al. 1996; Yin and Zhang 1997; Pan et al. 2012; Dong et al. 2018).

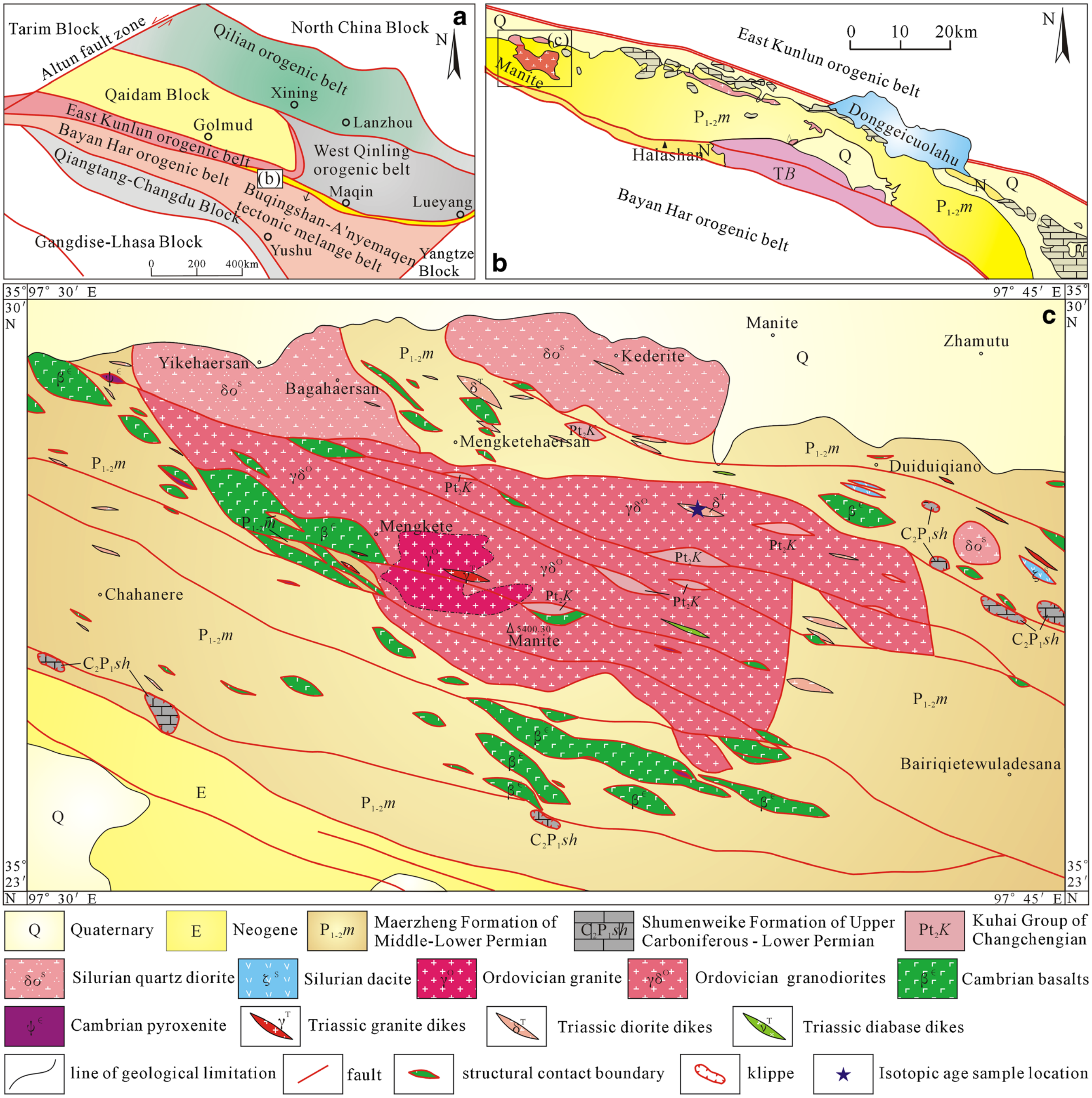

Fig. 1 **a** Geological map of the middle-western sections of the Central Orogenic Belt of China; **b** geological sketch map of the Buqingshan-A'nyemaqen tectonic mélange belt (BTMB) and its adjacent areas; **c** geological map of the BTMB, southern margin of the EKOB (modified from China University of Geosciences (Wuhan) Geological Survey 2000)

Controversy regarding the evolution process and geodynamic setting of BTMB remains. Xu et al. (2006b, c, d) suggest that the BTMB subduction–accretion complex is the product of subduction of the northern branch of the Paleo-Tethys oceanic crust. Other researchers have proposed that the East Kunlun orogenic belt (EKOB) and BTMB together form a large subduction–accretion–type tectonic mélange belt, and the paleo–ocean basin represented by the Buqinshan ophiolite continued to evolve from the Cambrian to the Early Triassic. The central of the East Kunlun and the Buqinshan ophiolites had accumulated together along the southern margin of the EKOB in the Middle and Late Triassic (Jiang et al. 1992, 2000; Wang et al. 1997b, 1999; Bian et al. 2001a, b, c, 2004, 2007; Li et al. 2007; Li et al. 2015a; Xiong et al. 2015; Liu et al. 2011a, b, c). To clarify the evolution of the BTMB, more research and data are needed and provided in this paper.

Due to their characteristic stability, zircons and their U–Pb ages are extremely useful in constraining the tectonic evolution of a region (Hartmann 2001; Wu et al. 2008; Wang et al. 2011; Zhang et al. 2015; Hoskin and Black 2000; Hoskin and Ireland 2000; Griffin et al. 2000; Belousova et al. 2002; Rubatto 2002; Hoskin and Schaltegger 2003; Hoskin 2005; Hanchar and Westrenen 2007). Previous studies mainly focused on the EKOB along the north side of the BTMB and obtained considerable evidence from zircon U–Pb geochronology (Chai et al. 1984; Harris et al. 1988; Chen et al. 2002a; Liu et al. 2004; Mo and Pan 2006; Sun et al. 2009; Chen et al. 2013a, b, c, 2017a, b, 2018a, b, c; Li et al. 2013a, b, 2017a, 2018a, b, 2019; Li et al. 2013c, 2018c; Chen et al. 2016; Deng et al. 2016; Hu et al. 2017; Zhang et al. 2017). These studies found granitoids with both Early Paleozoic ages in the BTMB (Liu et al. 2011a; Li et al. 2014a, 2015a, b; Li et al. 2014b, 2017b), as well as younger ones in the eastern section of the EKOB, dated at 230–256 Ma (Liu et al. 2004; Chen et al. 2013a, b, c, 2017a, 2018a, b, c; Ding et al. 2014; Chen et al. 2016; Li et al. 2018a). Late Triassic ages of granitoids have so far only been found in the Gerizhuotuo diorite (Li et al. 2013c). To expand the database on igneous rocks in the BTMB, we here analyze the petrology, geochronology, and geochemistry of intermediate–basic dikes in the BTMB. We also discuss the source and petrogenesis of the dikes, and made an attempt to provide new evidence for the Late Triassic tectonic evolution of the BTMB.

Geological background

The E-W striking BTMB discontinuously is more than 700 km long and approximately 10–20 km wide. It starts from Maqin in the east and extends across the Majixueshan and Tuosuohu to Buqingshan and southeast Heicigou to connect with the mafic–ultramafic rocks of Muzitage (Molnar et al. 1987; Burchfiel et al. 1989; Bian et al. 2004; Fig. 1a). To the north, the BTMB is separated from the East Kunlun and West Qinling orogens by the southern East Kunlun Fault, and to the south, it is separated from the Songpan–Bayan Har Orogen by the Changshitou Fault. The BTMB itself forms a suture zone between the Bayan Har and East Kunlun Blocks and is a product of two phases of ocean–continent subduction–collision in the Early and Late Paleozoic (Zhang et al. 1999). It also is part of the East Tethys Ocean tectonic domain (Jiang et al. 1992; Bian et al. 1999a, b, 2001c; Chen et al. 1999, 2000a, 2004; Zhu et al. 1999; Yang et al. 2004; Guo et al. 2007; Liu et al. 2011a, b, c; Pei et al. 2018).

The BTMB comprises the Lower–Middle Permian Maerzheng Formation ($P_{1-2}m$), including Early Paleozoic and Late Paleozoic ophiolites, Paleozoic rock mass, seamount basalts, and limestone (Liu et al. 2011b; Li et al. 2013c, 2014b, 2017b; Li et al. 2014a, 2015a, b; Pei et al. 2015, 2018; Yang et al. 2016; Pei et al. 2017). In the northern part of the ophiolite belt is the Middle Proterozoic Kuhai Group (Pt_2K), which comprises marble, biotite–quartz schist, gneiss, and amphibolite and constitutes the metamorphic basement rocks. A nappe composed of the Upper Carboniferous to Lower Permian Shumenweike Formation ($C_2P_{1-2}sh$), which primarily comprises carbonates with apparent reef affinities (Fig. 1b), covers the entire area.

The BTMB also includes various mafic to felsic dikes that intruded rock masses of various ages and diverse stratigraphy. The dikes intruded parallel to bedding or intersect it at an oblique angle. Their NW orientation appears fault controlled. The rock types primarily include diabase, diorite, granodiorite, granite, and syenogranite. According to the intersection relationships of the dikes, their relative intrusion order may be represented as diabase → diorite → granodiorite → granite → syenogranite. Indosinian dikes are widely distributed in the EKOB, indicating that the Indosinian magmatic event was widespread across the region.

Analytical methods

Petrographic sample preparation and microscopy

Thin sections of rocks were completed at the Laboratory of Mineralization and Dynamics of Chang'an University. During sample preparation, after cutting the rock sample, it is ground with different specifications of sandpaper. Then, the polished rock slab and the glass slide are dried in a preheated oven, and the surface of the rock block is attached to the glass slide using epoxy resin. After cooling, it was cut down to a thickness of 1 mm using a precision cutter and then ground to a light-transmission level (~ 30 μm), and polished with diamond paste and alumina for about 10 min each until the surface of the section was flat and free of mechanical scratches. Petrographic observation and photomicrography were performed using an ORTHOPLAN partial and reflective research microscope from Leitz, Germany.

LA–ICP–MS testing

One sample (MNT-21) of the diorite dike was evaluated for isotopic dating, whose geographic coordinates are N 35° 27′ 30.7″ and E 97° 39′ 42.3″ (Fig. 1).

Rock samples were crushed to 80–100 meshes using conventional methods and separated by flotation and electromagnetism techniques. Well-formed, crystal-shaped, and transparent zircons were handpicked using a binocular microscope. Zircon grains were mounted on a two-sided adhesive tape and fixed with colorless transparent epoxy resin until fully solidified; the surface was polished to expose the interior of the zircons. Cathodoluminescence (CL) microphotography images were taken with a Cameca electron probe X-ray micro-analyzer at the Institute of Geology and Geophysics, Chinese Academy of Sciences. The analysis voltage was 15 kV and the current was 19 nA.

The in situ U–Pb isotopic age analysis of zircons was carried out following the standard test procedure using an LA–ICP–MS at the State Key Laboratory of Continental Dynamics, Northwest University. The analysis instruments were an Elan 6100DRC Type Quadrupole Perch Mass Spectrograph and a Geolas200M excimer laser ablation system (193 nm, Geolas200M, Lambda Physic). The facula beam's diameter of laser ablation was 30 μm, and the depth of laser ablation samples was 20–30 μm. For the calculation of zircon ages, the international standard zircon 91500 was used as an external standard; for the element content analysis, the artificial synthetic silicate glass NIST SRM610 of the American National Standard Substance Bureau was adopted as an external standard. ^{29}Si was used as the internal standard element. The isotopic ratio and element content data were analyzed with GLITTER (ver. 4.0, Macquarie University) software, general plumbum adjustment was conducted using the Andersen software (Andersen 2002), and age calculation and concordia diagram drafting were completed using ISOPLOT (3.0 edition) (Ludwig 2003). The detailed experimental principles, technological process, and instrumentation parameters were the same as those reported by Yuan et al. (2003, 2004).

Geochemical analysis

Nine samples were selected for the analysis of major and trace elements. The samples were ground to 200 meshes and the major and trace elements were determined by the State Key Laboratory of Lithosphere Evolution, Institute of Geology and Geophysics, Chinese Academy of Sciences. The major elements were tested using the method of X-ray fluorescence spectrometry (XRF–1500). To determine the content of oxide, a sheet glass made of 0.5-g samples and 5 g lithium tetraborate was tested using the Shimadzu XRF–1500, with a precision of > 2–3%. The contents of the trace and rare earth elements (REEs) were analyzed by ICP–MS (ElementII). The samples were prepared using the acid-solubility method, which has an analytic precision of > 10% (according to the national standards GSR–1 and GSR–2), but the precision is > 5% when the element content is > 10 ppm. The detailed analysis methods were described by Chen et al. (2000b, 2002b).

Results

Petrography

The sampled dikes can be classified as diabase and diorite. The diabase, gray–black and fine-grained with typical diabasic texture (Fig. 2a, b), is composed primarily of plagioclase (50–60%), pyroxene (± 20%), and minor amounts of hornblende, biotite, and opaque minerals (8–10%). The diorite, dark–gray and fine- to particle-grained with hypidiomorphic granular texture, is composed primarily of plagioclase (65–70%), hornblende (± 20%), quartz (3–5%), and biotite (5–8%) with accessory amounts of zircon, apatite, and magnetite (Fig. 2c). Plagioclase is the most abundant phenocryst and commonly has polysynthetic twins (Fig. 2d). Biotite and hornblende are dark–green or brownish. Some euhedral plagioclase grains are included within quartz crystals (Fig. 2d).

Whole-rock chemistry

The intermediate–basic dikes of BTMB samples have relatively low concentrations of SiO_2 (51.96–59.33 wt%), K_2O (1.45–2.70 wt%), K_2O+Na_2O (4.00–5.29 wt%), TiO_2 (0.30–0.60 wt%), Al_2O_3 (10.49–13.95 wt%), and high concentrations of total Fe_2O_3 (6.29–8.68 wt%), MgO (5.16–11.79 wt.%), and CaO (5.86–10.15 wt%) (Table 1). All samples exhibit subalkaline trends in a total alkali–silica (TAS) diagram (Fig. 3), and the intermediate dikes plot in the andesite and basalt fields.

From the characteristics of the intermediate–basic dikes of the BTMB in Table 1, we can conclude that the concentration of REEs are 80.23–189.19 ppm, and the ratios of light RREs (LREEs) to heavy RREs (HREEs) (LREE/HREE = 6.53–13.15), with $(La/Yb)_N$ = 5.62–19.16, $(La/Sm)_N$ = 2.67–3.35. The HREE losses may be due to residual garnet and amphibole at the source (Patino–Douce and Johnston 1991). Chondrite-normalized REE patterns display an incline to the right (Fig. 4a). The diorite samples generally show similar patterns, with differences in abundance and weak negative Eu anomalies (δEu = 0.50–1.10) that may have been induced by the differentiation of plagioclases and K-feldspars.

The intermediate–basic dikes are characterized by high Rb, Th, and low Rb/Sr ratios (0.14–0.37); Ra/Ba ratios (0.04–0.28); and high K/Rb ratios (75.52–355.14) (Table 1). On the primitive mantle-normalized spidergram (Fig. 4b), they are characterized by enrichment in LILEs relative to HFSEs, showing notable negative Ta, Nb, Sr, P, and Ti anomalies and positive U, Ce, Nd, Sm, and Hf anomalies. The diorite and diabase dikes show different characteristics, with anomalous Zr, Th, Rb, and Ba.

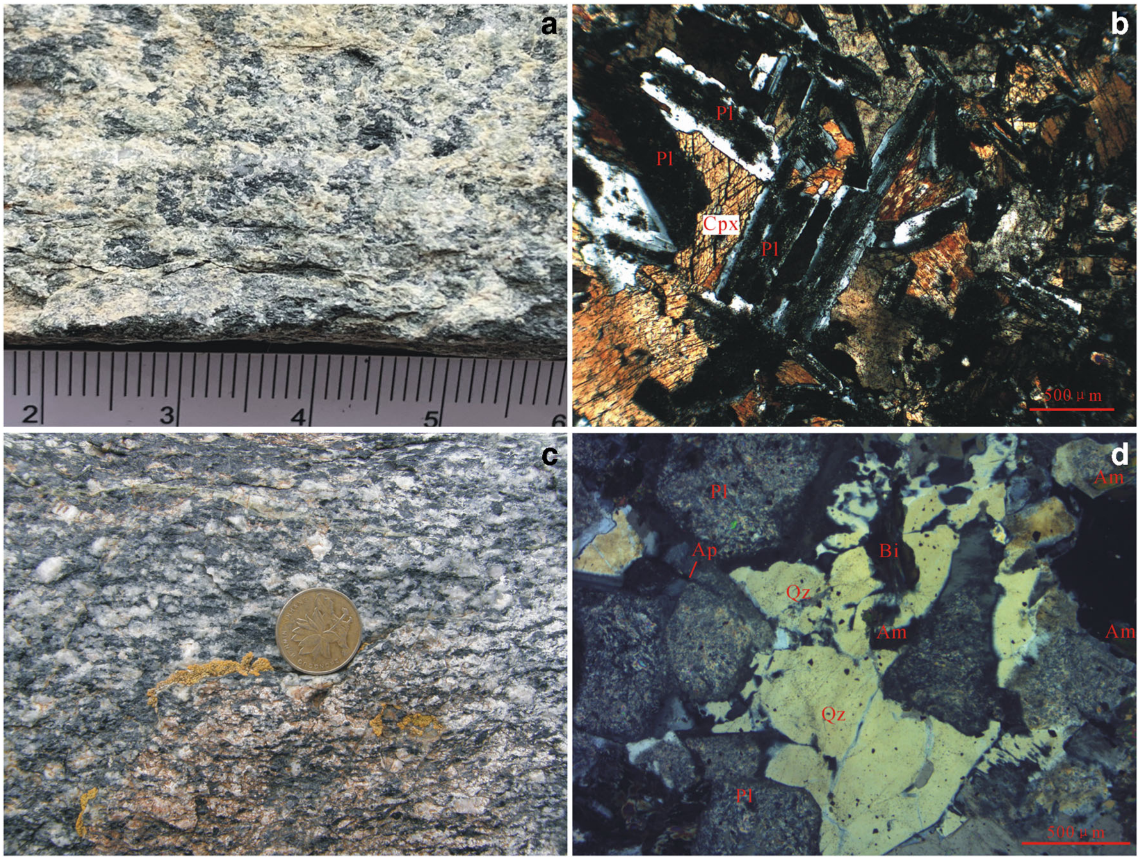

Fig. 2 **a**, **b** Field photographs and microscopic photos of the diabase. **c**, **d** Field photographs and microscopic photos of the diorite in the BTMB, southern margin of the EKOB Am, amphibole; Ap, apatite; Bi, biotite; Cpx, clinopyroxene; Pl, plagioclase; Qz, quartz; **b**, **d**, crossed polarizers, 20 times

Zircon U–Pb ages

Zircons from the diorite dike (sample MNT-21) are euhedral to subhedral (Fig. 5a) with lengths in the range 100–250 μm and width/length ratios of 1:1 to 1:10.

Thirty zircon analyses yielded Th concentrations in the range 70–1267 ppm and U concentrations in the range 103–1979 ppm (Table 2). A plot of total U versus Th shows a good linear relation (Fig. 6a). The chondrite-normalized REE patterns (Sun and McDonough 1989) (Fig. 6b) indicate that the zircons are depleted in LREEs relative to HREEs with positive Ce anomalies and negative Eu anomalies (δEu = 0.13–0.48) (Table 3).

Except for the six apparent discordia data (e.g., analysis spot numbers 002, 005, 015, 022, 023, 029) and captured or inherited zircon ages (e.g., analysis spot numbers 020, 627 Ma) (Table 2), the remnant 23 zircon grains form a single population (Fig. 5b). The 23 testing points are perfectly concordant among ^{206}Pb/^{238}U and ^{207}Pb/^{235}U ages, the concordia age of 204 ± 2 Ma (MSWD = 0.46) (Fig. 5b), and the ^{206}Pb/^{238}U weighted average age of 205 ± 1 Ma (MSWD = 0.88) (Fig. 5c). We interpret this to represent the Late Triassic (Rhaetian) crystallization age of the diorite dike.

Discussion

Formation time of the dikes

The zircons analyzed were taken from the diorite dike (sample MNT-21) in the BTMB. The majority of these zircons show oscillatory zoning structures, indicating that they are magmatic zircons (Belousova et al. 2002; Wu and Zheng 2004; Siebel et al. 2005). This is corroborated by the high Th/U ratios (0.47–2.43) (Table 2), indicating a magmatic origin (Vavra et al. 1999; Claesson et al. 2000; Wu and Zheng 2004). A plot of total U versus Th shows a good linear relation, which also is a feature typical of magmatic zircons (Fig. 6a; Vavra et al. 1999; Claesson et al. 2000; Wu and Zheng 2004). The chondrite-normalized (Sun and McDonough 1989) REE

Table 1 Major element data components (wt%) and trace element abundance (ppm) for the intermediate–basic dikes in the BTMB, southern margin of the EKOB

Sample	MNT/10	MNT/12-1	MNT/12-2	MNT/13	MNT/15	MNT/21	MNT/22-1	MNT/22-2	MNT/23
SiO_2	51.96	54.44	54.35	54.10	53.47	59.17	58.08	58.80	59.33
TiO_2	0.35	0.31	0.30	0.31	0.31	0.60	0.59	0.60	0.56
Al_2O_3	11.94	11.45	11.14	10.49	10.58	13.95	12.54	12.59	12.76
$Fe_2O_3^T$	8.68	7.35	7.49	7.66	7.72	6.44	6.95	6.58	6.29
FeO	5.75	4.96	5.06	5.35	5.39	4.31	5.30	4.96	4.63
MnO	0.17	0.13	0.13	0.15	0.16	0.15	0.18	0.17	0.16
MgO	11.79	9.92	10.11	10.78	11.18	5.16	5.94	5.69	5.55
CaO	9.01	9.06	8.97	9.97	10.15	5.86	6.80	6.49	6.28
Na_2O	2.27	2.63	2.56	2.63	2.55	3.18	3.22	3.10	3.11
K_2O	1.76	2.61	2.70	1.77	1.45	2.02	1.99	1.97	2.17
P_2O_5	0.20	0.20	0.20	0.20	0.20	0.22	0.22	0.23	0.23
LOI	1.46	1.72	1.86	1.78	2.09	3.10	3.33	3.64	3.39
Total	99.59	99.82	99.81	99.84	99.86	99.85	99.84	99.86	99.83
Ti	2098.25	1876.12	1807.78	1859.87	1829.03	3597.00	3559.94	3584.85	3379.91
K	7304.00	10,830.67	11,199.57	7344.35	6006.70	8383.00	8274.81	8160.22	9018.91
P	436.20	443.46	432.70	434.43	435.23	479.82	489.36	501.96	509.74
Li	6.99	3.44	3.58	3.04	4.59	19.00	14.72	18.16	12.84
Be	0.54	1.11	1.09	1.25	1.30	1.50	2.65	2.44	2.26
Sc	48.60	9.43	13.00	10.07	13.36	17.00	5.29	5.71	4.13
V	247.00	195.80	205.50	212.60	215.50	98.20	117.20	113.20	109.60
Cr	555.00	438.00	523.80	444.10	510.60	275.00	363.80	285.50	336.30
Co	42.60	37.96	38.35	36.37	38.15	21.10	22.70	21.75	22.03
Ni	142.00	111.00	118.20	120.50	128.60	58.80	86.44	82.93	84.74
Cu	42.80	34.72	34.26	52.26	32.84	47.20	50.65	50.89	59.84
Zn	56.00	39.63	44.23	47.42	53.00	66.90	74.33	68.40	69.65
Ga	12.00	8.48	9.49	7.92	8.79	16.60	13.93	12.50	13.68
Rb	55.10	33.26	38.14	20.68	19.36	111.00	56.61	66.38	59.38
Sr	178.54	153.10	180.50	131.00	136.60	299.00	219.20	274.70	262.20
Zr	66.94	81.91	79.93	75.76	76.41	306.17	130.10	191.10	117.00
Nb	5.12	5.56	5.58	4.77	4.60	33.60	36.76	34.79	32.26
Mo	19.40	0.99	1.31	13.45	14.14	0.29	0.58	0.36	0.32
In	0.05	0.03	0.04	0.04	0.05	0.08	0.09	0.07	0.07
Cs	0.69	0.23	0.38	0.22	0.19	3.87	1.47	1.82	1.47
Ba	698.00	734.50	786.30	604.90	536.20	459.00	223.50	233.30	266.60
Hf	0.88	2.85	2.84	2.64	2.69	2.36	4.99	6.62	4.49
Ta	0.27	0.56	0.54	0.32	0.35	2.44	3.09	3.01	2.50
W	0.12	0.28	0.15	0.31	0.23	0.71	0.86	0.97	0.88
Tl	0.30	0.32	0.34	0.24	0.18	0.45	0.36	0.38	0.39
Pb	6.18	8.31	8.87	8.41	6.85	14.50	18.36	11.72	14.16
Bi	0.10	0.16	0.17	0.10	0.08	0.08	0.09	0.07	0.10
Th	7.77	5.30	5.82	5.22	5.50	21.50	12.81	8.65	7.53
U	1.25	2.05	2.55	1.54	1.41	2.47	3.55	3.00	3.40
La	20.30	16.91	17.07	16.18	15.67	32.80	21.74	18.46	14.52
Ce	40.30	36.59	36.57	34.45	34.62	70.40	77.24	64.64	59.54
Pr	5.25	3.95	4.09	4.05	4.00	9.94	6.78	6.65	4.68
Nd	20.90	14.96	15.80	15.53	15.63	41.40	25.97	26.53	17.82

Table 1 (continued)

Sample	MNT/10	MNT/12-1	MNT/12-2	MNT/13	MNT/15	MNT/21	MNT/22-1	MNT/22-2	MNT/23
Sm	3.91	2.66	2.86	2.84	2.84	7.93	4.56	4.97	3.11
Eu	1.04	0.89	0.99	0.91	0.89	1.61	0.72	0.82	0.61
Gd	3.17	2.41	2.65	2.54	2.61	6.61	4.22	4.41	3.01
Tb	0.48	0.29	0.33	0.32	0.33	1.20	0.59	0.63	0.40
Dy	2.44	1.31	1.55	1.45	1.52	6.65	2.98	3.15	1.96
Ho	0.44	0.24	0.28	0.26	0.28	1.31	0.57	0.59	0.37
Er	1.26	0.71	0.85	0.79	0.82	3.85	1.73	1.77	1.13
Tm	0.18	0.09	0.11	0.11	0.11	0.66	0.25	0.26	0.16
Yb	1.22	0.63	0.78	0.73	0.78	4.19	1.66	1.75	1.10
Lu	0.19	0.10	0.12	0.10	0.12	0.65	0.25	0.26	0.16
Y	12.00	5.41	6.69	5.96	6.43	37.40	12.82	13.32	8.34
ΣREE	101.08	81.73	84.05	80.25	80.23	189.19	149.25	134.90	108.56
LREE	91.70	75.95	77.39	73.96	73.65	164.08	137.00	122.07	100.28
HREE	9.38	5.78	6.66	6.29	6.58	25.11	12.25	12.83	8.28
LREE/HREE	9.77	13.15	11.61	11.76	11.20	6.53	11.19	9.52	12.11
$(La/Yb)_N$	11.94	19.16	15.78	15.90	14.36	5.62	9.38	7.58	9.43
δEu	0.90	1.07	1.10	1.03	1.00	0.68	0.50	0.54	0.61

LOI loss on ignition; subscript N-chondrite-normalized value; $Fe_2O_3^T$ = all Fe calculated as Fe_2O_3; $\delta Eu = (Eu)_N/[(Sm)_N \times (Gd)_N]^{1/2}$; chondrite REE values are after Sun and McDonough 1989

patterns (Fig. 6b) indicate that the zircons are depleted in LREEs relative to HREEs. The zircons display positive Ce anomalies ($\delta Ce = 1.02–79.30$) and negative Eu anomalies ($\delta Eu = 0.13–0.48$) (Table 3), which are consistent with characteristics of crustal magmatic zircons (Hoskin and Schaltegger 2003).

Cathodoluminescence (CL) imaging of sample MNT-21 shows the complete zircon morphology, obvious oscillatory zonal structure, and Th/U values of all the analysis points greater than 0.1, demonstrating magmatic zircon characteristics (Tapia–Fernandez et al. 2017). The 23 analysis points obtained a relatively consistent $^{206}Pb/^{238}U$ apparent age, with the $^{206}Pb/^{238}U$ weighted average age of 205 ± 1 Ma, considered to be the crystallization age of the diorite dike.

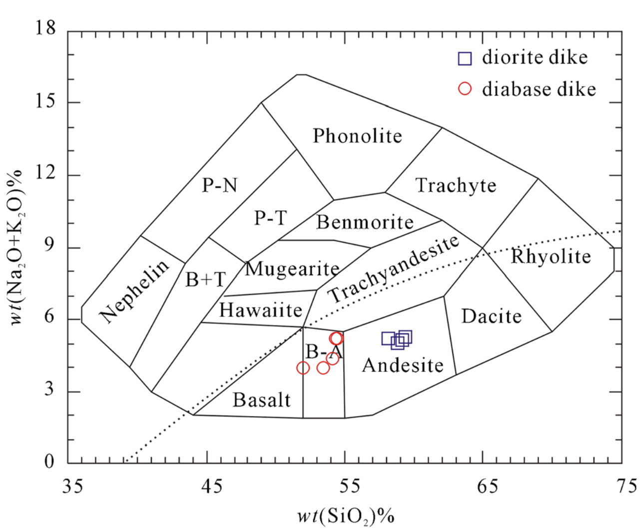

Fig. 3 TAS diagrams for the intermediate–basic dikes (after Rickwood 1989) in the BTMB, southern margin of the EKOB

Petrogenesis

The diabase dikes are relatively enriched in LREE and LREE, with Nb and Ta negative anomalies, and have relatively low Nb/U ratios (2.19–4.10) and high Zr/Nb ratios (13.07–16.61) that are significantly different from those of the standard OIB (Nb/U = 47.06 and Zr/Nb = 5.83, according to Sun and McDonough 1989). The diabase dikes in the BTMB have obvious Nb, Ta, and Ti negative anomalies, which reflect the geochemical characteristics of island-arc basalt, suggesting either crustal contamination or metasomatism by subduction fluid (Green and Pearson, 1987; Rollinson 1993; Green 1995; Barth et al. 2000). High primitive mantle-normalized $(Th/Nb)_N$ ratios (≫ 1, Saunders et al. 1992) and low Nb/La ratios (< 1, Kieffer et al. 2004) are two reliable trace element indicators for crustal contamination. The BTMB diabase dikes do have high $(Th/Nb)_N$ ratios (7.89–12.56) and low Nb/La ratios (0.25–0.33), suggesting crustal contamination. The diorite dike shows characteristics that are opposite to those of the diabase dikes, with lower $(Th/Nb)_N$ ratios (1.93–5.30) and

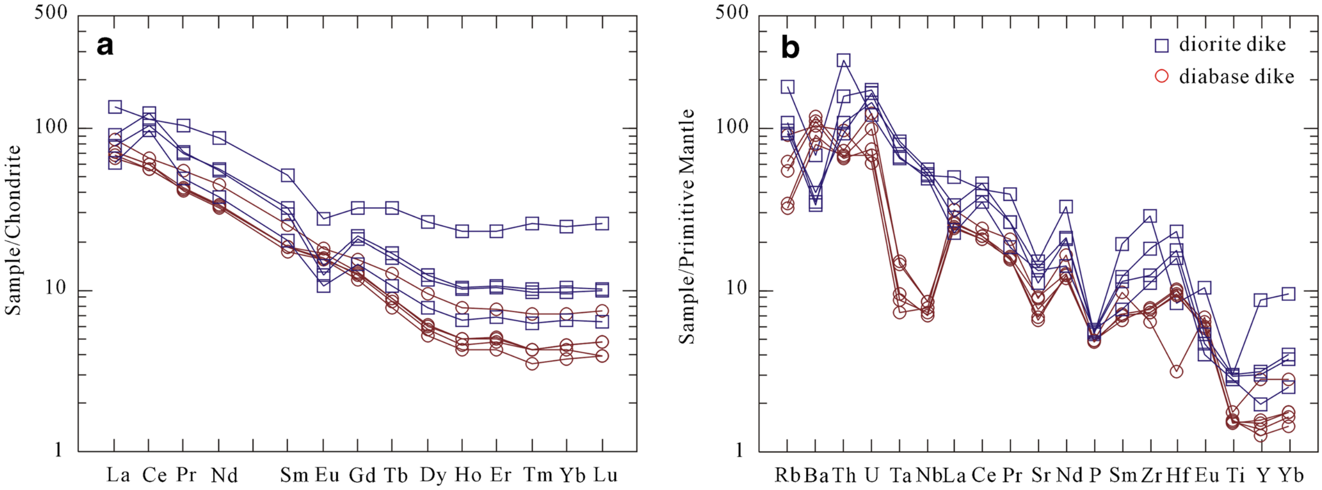

Fig. 4 **a** Chondrite-normalized REE patterns (chondrite data for normalization taken from Sun and McDonough 1989). **b** Trace element spider diagram (primitive mantle data for normalization taken from McDonough and Sun 1995) for the intermediate–basic dikes in the BTMB, southern margin of the EKOB

higher Nb/La ratios (1.02–2.22). This contrast suggests that the diorite and diabase magmas may have had different source areas.

Magma temperatures

High-temperature and high-pressure experiments indicate that the Ti content in zircon is closely related to temperature, producing a logarithmically linear relationship. That is, the zircon Ti thermometer has an empirical formula temperature estimation whose error is generally no more than 10 °C. This thermometer is simple and practical, so it is utilized by many researchers for great practicality (Watson et al. 2006; Zhao 2010; Gao and Zheng 2011).

We obtained data for 30 measuring points in the BTMB diorite dike (MNT-21), among which 23 are effective points used in our calculations. Plugging the Ti content measured in the sample zircon into the formula, the lowest temperature of

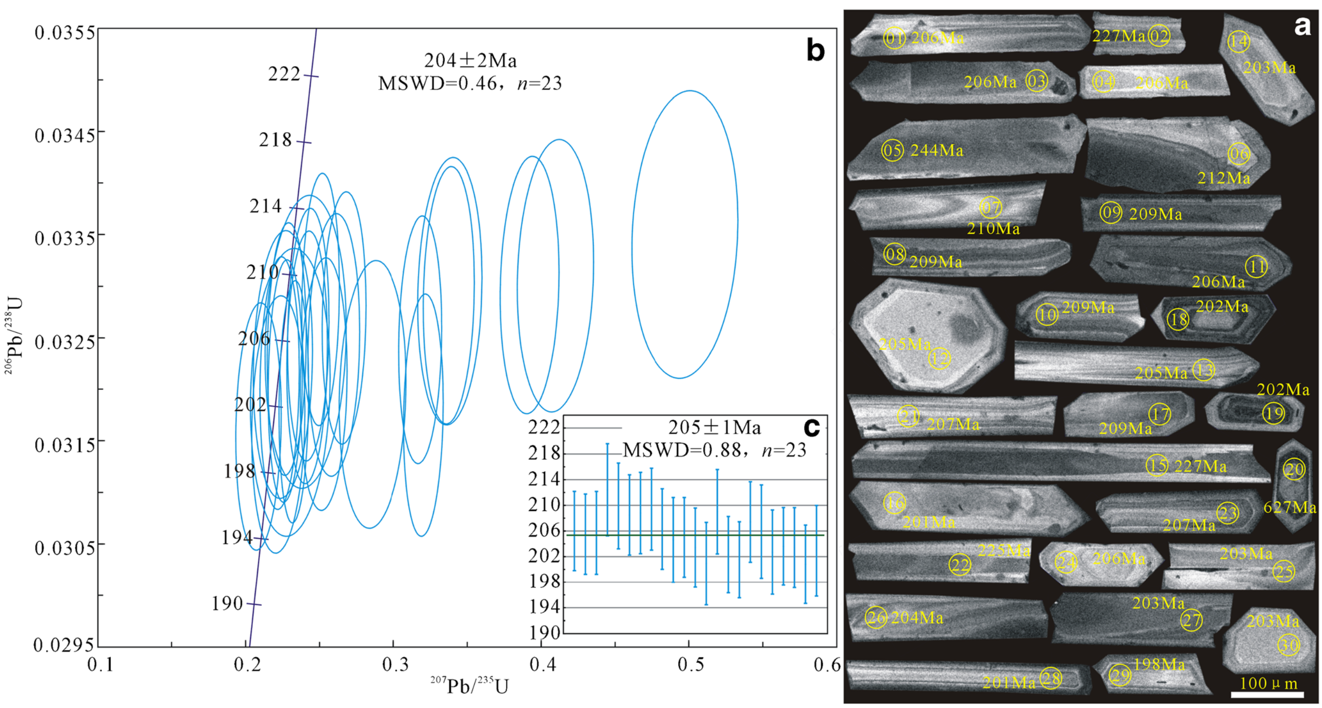

Fig. 5 **a** CL images and ages of single zircon U–Pb of diorite dike (the yellow circle is the sample test point position). **b**, **c** LA-ICP-MS zircon U–Pb concordia diagram of diorite dike in the BTMB, southern margin of the EKOB

Table 2 LA-ICP-MS zircon U–Pb analytic data and Ti geological temperature calculation for diorite dikes in the BTMB, southern margin of the EKOB

Analysis spot	Content (ppm)			Th/U	Isotope ratios								Apparent age (Ma)						Zircon temperature (°C)
	Pb	Th	U		$^{207}Pb/^{206}Pb$	1σ	$^{207}Pb/^{235}U$	1σ	$^{206}Pb/^{238}U$	1σ	$^{208}Pb/^{232}Th$	1σ	$^{207}Pb/^{206}Pb$	1σ	$^{207}Pb/^{235}U$	1σ	$^{206}Pb/^{238}U$	1σ	
MNT-21-01	65	455	448	1.02	0.0711	0.0023	0.3182	0.0059	0.0325	0.0005	0.0118	0.0002	959	64	281	5	206	3	961
MNT-21-02	72	551	451	1.22	0.0713	0.0024	0.3522	0.0072	0.0358	0.0006	0.0125	0.0002	966	67	306	5	227	3	728
MNT-21-03	40	276	265	1.04	0.0510	0.0018	0.2278	0.0054	0.0324	0.0005	0.0102	0.0002	241	80	208	5	206	3	782
MNT-21-04	44	371	295	1.26	0.0581	0.0022	0.2596	0.0071	0.0324	0.0005	0.0102	0.0002	532	82	234	6	206	3	764
MNT-21-05	46	544	269	2.03	0.0889	0.0029	0.4722	0.0093	0.0385	0.0006	0.0085	0.0001	1402	62	393	6	244	4	880
MNT-21-06	19	114	135	0.84	0.1077	0.0043	0.4973	0.0147	0.0335	0.0006	0.0154	0.0003	1761	72	410	10	212	4	804
MNT-21-07	42	272	271	1.00	0.0898	0.0033	0.4096	0.0105	0.0331	0.0005	0.0141	0.0002	1421	69	349	8	210	3	837
MNT-21-08	63	513	434	1.18	0.0553	0.0019	0.2507	0.0052	0.0329	0.0005	0.0106	0.0001	425	73	227	4	209	3	752
MNT-21-09	64	496	416	1.19	0.0744	0.0025	0.3375	0.0071	0.0329	0.0005	0.0117	0.0002	1052	66	295	5	209	3	780
MNT-21-10	36	213	233	0.91	0.0862	0.0029	0.3922	0.0081	0.0330	0.0005	0.0142	0.0002	1342	64	336	6	209	3	981
MNT-21-11	50	195	350	0.56	0.0541	0.0019	0.2424	0.0057	0.0325	0.0005	0.0113	0.0002	373	78	220	5	206	3	751
MNT-21-12	15	70	103	0.68	0.0507	0.0023	0.2252	0.0082	0.0322	0.0005	0.0107	0.0002	226	101	206	7	205	3	785
MNT-21-13	77	650	538	1.21	0.0542	0.0019	0.2416	0.0056	0.0323	0.0005	0.0104	0.0002	381	77	220	5	205	3	732
MNT-21-14	41	273	276	0.99	0.0505	0.0018	0.2230	0.0054	0.0321	0.0005	0.0101	0.0002	216	81	204	5	203	3	765
MNT-21-15	103	891	637	1.40	0.1081	0.0034	0.5329	0.0090	0.0358	0.0005	0.0154	0.0002	1767	56	434	6	227	3	745
MNT-21-16	32	228	228	1.00	0.0509	0.0022	0.2222	0.0073	0.0317	0.0005	0.0099	0.0002	236	95	204	6	201	3	768
MNT-21-17	45	257	288	0.89	0.0745	0.0028	0.3383	0.0089	0.0330	0.0005	0.0126	0.0002	1054	74	296	7	209	3	832
MNT-21-18	115	322	685	0.47	0.0529	0.0017	0.2326	0.0041	0.0319	0.0005	0.0107	0.0002	326	70	212	3	202	3	702
MNT-21-19	320	1267	1979	0.64	0.0732	0.0023	0.3204	0.0055	0.0318	0.0005	0.0099	0.0001	1019	62	282	4	202	3	702
MNT-21-20	414	851	1059	0.80	0.1102	0.0034	1.5511	0.0239	0.1021	0.0015	0.0341	0.0005	1803	54	951	10	627	9	748
MNT-21-21	64	579	424	1.36	0.0592	0.0021	0.2666	0.0061	0.0327	0.0005	0.0099	0.0001	573	74	240	5	207	3	733
MNT-21-22	27	128	153	0.84	0.0965	0.0033	0.4728	0.0099	0.0355	0.0006	0.0165	0.0003	1557	62	393	7	225	3	954
MNT-21-23	57	472	477	0.99	0.0784	0.0028	0.3533	0.0083	0.0327	0.0005	0.0117	0.0002	1157	69	307	6	207	3	876
MNT-21-24	25	393	162	2.43	0.0538	0.0029	0.2406	0.0112	0.0325	0.0006	0.0113	0.0003	362	117	219	9	206	4	760
MNT-21-25	39	232	247	0.94	0.0649	0.0028	0.2860	0.0093	0.0320	0.0005	0.0114	0.0002	772	87	255	7	203	3	725
MNT-21-26	68	589	451	1.31	0.0513	0.0017	0.2268	0.0047	0.0321	0.0005	0.0107	0.0002	254	76	208	4	204	3	731
MNT-21-27	61	492	477	1.03	0.0572	0.0021	0.2528	0.0065	0.0321	0.0005	0.0115	0.0002	499	80	229	5	203	3	718
MNT-21-28	68	546	465	1.17	0.0479	0.0019	0.2088	0.0063	0.0316	0.0005	0.0106	0.0002	92	94	193	5	201	3	730
MNT-21-29	81	656	492	1.33	0.0678	0.0033	0.2909	0.0118	0.0312	0.0006	0.0122	0.0003	861	99	259	9	198	4	754
MNT-21-30	17	89	112	0.79	0.0522	0.0029	0.2302	0.0110	0.0320	0.0006	0.0111	0.0003	296	122	210	9	203	4	778

Ti geological temperature is T (°C) = (5080 ± 30) / [(6.01 ± 0.03)-log (Ti)] − 273 (Watson et al. 2006)

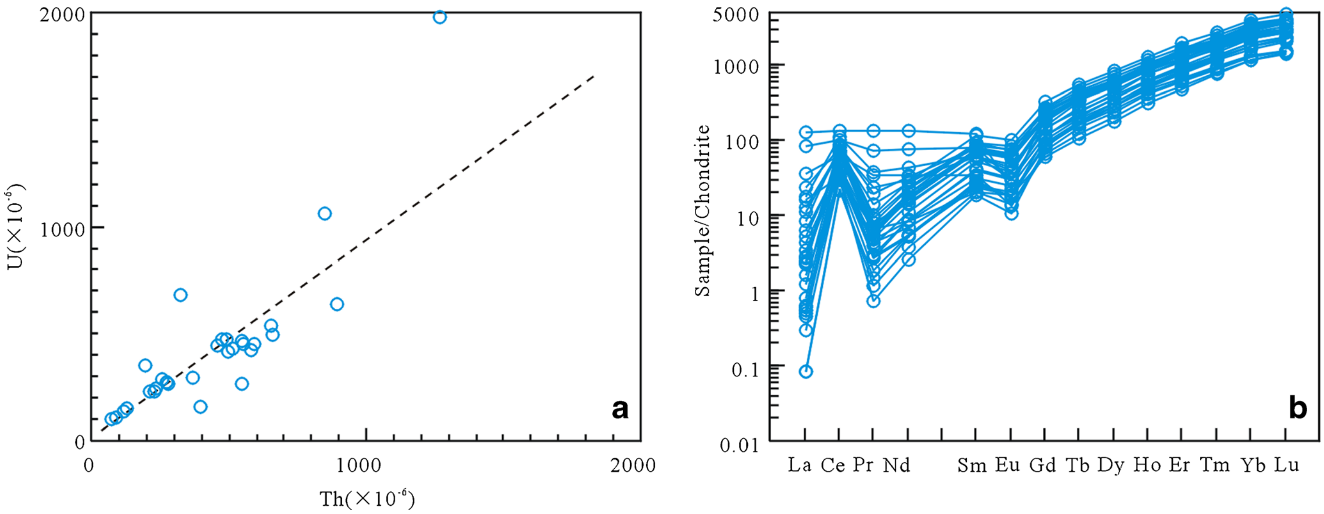

Fig. 6 Th-U diagrams and chondrite-normalized REE patterns (chondrite data for normalization taken from Sun and McDonough 1989) of Zircon for diorite dike in the BTMB, southern margin of the EKOB

Table 3 Zircon trace element (ppm) analytical results of diorite dikes in the BTMB, southern margin of the EKOB

Analysis spot	La	Ce	Pr	Nd	Sm	Eu	Gd	Tb	Dy	Ho	Er	Tm	Yb	Lu	ΣREE	δEu	δCe
MNT-21-01	2.67	42.97	0.77	6.84	9.06	2.55	38.33	13.09	143.46	52.58	228.67	52.04	506.35	91.63	1191.01	0.36	7.33
MNT-21-02	0.19	38.27	0.53	7.74	10.55	3.55	42.04	13.42	141.57	50.61	218.97	49.76	487.29	90.20	1154.69	0.45	29.78
MNT-21-03	0.13	20.41	0.48	6.57	9.10	2.24	40.13	13.84	150.88	53.22	222.06	46.44	425.06	74.37	1064.93	0.30	19.90
MNT-21-04	0.65	28.29	0.56	7.61	11.54	3.48	55.78	18.32	190.14	65.74	273.66	55.65	511.71	89.60	1312.73	0.35	11.53
MNT-21-05	5.57	48.77	2.24	13.60	9.32	2.70	29.97	9.41	99.33	35.61	151.26	34.40	329.55	61.01	832.74	0.45	3.39
MNT-21-06	0.14	18.46	0.18	2.61	4.20	1.04	19.19	6.63	73.35	26.79	110.23	24.73	226.93	38.99	553.48	0.30	27.90
MNT-21-07	1.04	23.25	0.45	3.86	4.70	1.42	20.70	7.15	80.17	31.20	134.36	31.63	304.44	57.67	702.04	0.37	8.39
MNT-21-08	0.29	43.11	0.67	9.11	11.23	3.72	42.16	13.62	143.63	51.44	220.47	50.11	493.75	91.51	1174.82	0.46	23.87
MNT-21-09	0.53	43.61	0.56	7.66	10.40	3.26	40.86	13.58	145.37	52.37	229.25	51.42	501.18	91.43	1191.48	0.42	19.59
MNT-21-10	1.51	27.75	0.42	3.25	3.82	1.16	17.30	6.15	71.52	28.09	125.61	29.22	278.75	51.48	646.02	0.37	8.57
MNT-21-11	0.82	20.80	0.26	2.46	4.30	1.05	22.32	8.68	105.04	42.87	186.31	42.82	405.59	72.73	916.05	0.26	11.11
MNT-21-12	0.02	13.57	0.11	1.78	3.18	0.82	15.03	5.37	60.40	23.20	101.09	22.55	213.90	39.59	500.61	0.30	79.30
MNT-21-13	0.68	43.82	0.76	10.34	12.96	4.37	47.74	14.95	155.33	55.50	238.44	53.94	537.92	98.74	1275.49	0.48	14.95
MNT-21-14	0.15	23.76	0.38	5.23	8.06	2.21	36.91	12.79	140.40	50.87	217.39	46.45	435.17	75.61	1055.39	0.33	24.07
MNT-21-15	0.59	52.95	0.95	13.13	17.57	5.96	66.92	20.88	209.86	73.62	315.97	68.81	681.54	121.69	1650.45	0.47	17.25
MNT-21-16	0.07	20.24	0.28	4.03	6.28	1.80	28.35	10.09	115.98	43.72	187.77	40.85	386.53	68.92	914.91	0.35	35.14
MNT-21-17	1.23	31.87	0.27	2.55	3.55	1.06	17.08	6.32	73.61	29.97	132.07	31.60	305.24	56.45	692.87	0.34	13.50
MNT-21-18	0.39	18.15	0.07	1.18	2.84	0.60	16.20	6.52	77.37	30.95	136.15	32.02	304.34	53.15	679.93	0.21	27.20
MNT-21-19	19.83	60.68	6.87	35.99	12.44	1.73	31.85	11.98	150.64	58.07	270.44	61.65	617.63	107.08	1446.88	0.25	1.27
MNT-21-20	30.87	82.44	12.68	62.14	18.82	1.30	46.86	15.99	156.31	50.47	197.17	44.40	420.86	73.85	1214.16	0.13	1.02
MNT-21-21	2.97	44.64	1.35	12.45	12.02	3.84	41.16	12.93	133.31	47.03	201.30	46.37	459.88	83.09	1102.34	0.47	5.47
MNT-21-22	3.91	19.68	0.64	3.88	3.05	1.08	12.07	4.03	45.00	17.65	79.72	19.08	193.46	37.51	440.76	0.47	3.05
MNT-21-23	4.29	66.93	3.62	20.40	9.64	1.72	24.21	7.77	89.24	35.36	156.90	37.85	375.35	67.50	900.78	0.33	4.16
MNT-21-24	8.62	38.73	3.26	15.72	5.18	0.76	13.28	4.58	51.78	19.86	88.05	20.53	196.80	35.32	502.47	0.27	1.79
MNT-21-25	0.11	25.05	0.26	4.18	5.94	1.76	23.98	8.14	90.62	33.95	147.12	34.32	334.93	60.56	770.93	0.39	35.63
MNT-21-26	0.13	37.74	0.60	9.00	13.74	4.75	53.41	17.08	172.58	60.70	257.17	58.37	572.22	97.65	1355.14	0.47	32.66
MNT-21-27	1.99	51.79	1.89	15.42	12.36	3.34	40.93	12.62	134.85	47.57	198.75	45.37	448.80	75.15	1090.84	0.41	6.54
MNT-21-28	0.12	40.00	0.56	8.23	11.76	3.90	44.35	14.16	149.72	52.69	223.71	51.40	521.64	89.67	1211.91	0.46	38.41
MNT-21-29	0.57	49.84	0.86	11.12	13.84	4.28	49.99	15.45	162.69	57.78	244.82	55.99	555.54	95.07	1317.83	0.44	17.58
MNT-21-30	0.02	13.34	0.14	2.44	4.04	1.05	17.83	6.03	66.12	24.58	104.17	23.36	220.89	38.54	522.55	0.32	67.00

Subscript N-chondrite-normalized value; $\delta Eu = Eu_N/(Sm_N \times Gd_N)^{1/2}$; $\delta Ce = Ce_N/(La_N \times Pr_N)^{1/2}$. Chondrite REE values are after Sun and McDonough 1989

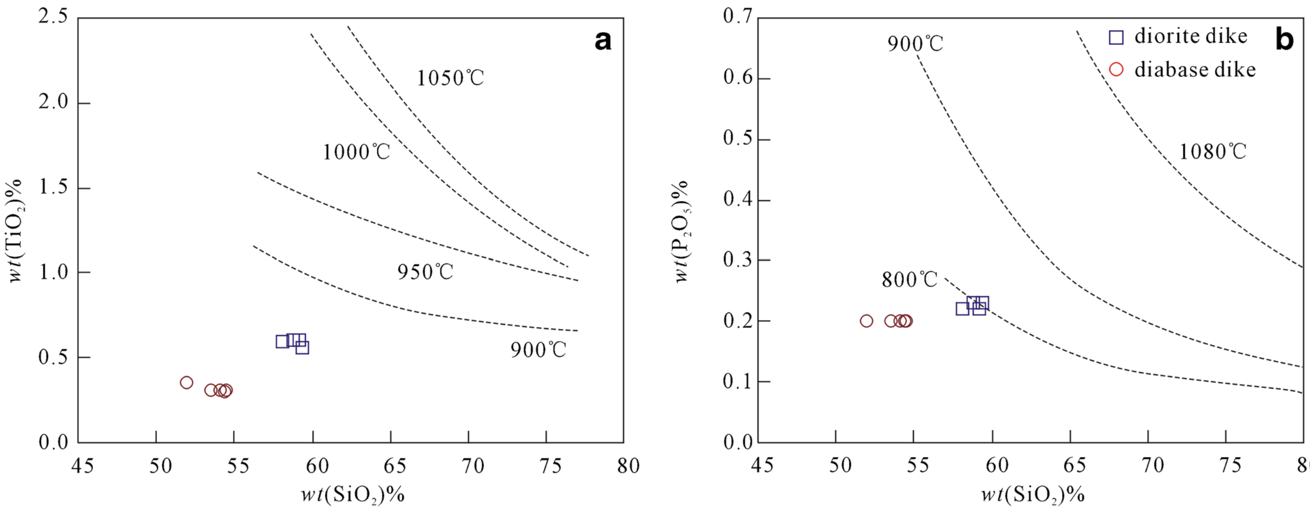

Fig. 7 **a** TiO_2-SiO_2 (after Harrison and Watson 1984) and **b** P_2O_5–SiO_2 (after Green and Pearson 1986) diagrams for diorite dike in the BTMB, southern margin of the EKOB

the intermediate–basic dikes in BTMB ranges from 702 to 981 °C, averaging ~ 777 °C. TiO_2–SiO_2 and P_2O_5–SiO_2 geothermometric measurements also verify that the formation temperature of the diorite dike is ~ 800 °C (Fig. 7a, b), confirming that they were formed in a high-temperature environment.

Tectonic setting

Heat flow at an extremely high temperature is required to melt large amounts of mafic rocks (England and Thompson 1986; Thompson and Connolly 1995). However, in general, this condition holds only in the tectonic setting represented by continental collision → continental crust thickening → crustal extension and thinning → asthenosphere uplift (Han et al. 2000; Vanderhaeghe 2009; Bea 2012; Hasterok and Webb 2017). The intermediate–basic dikes in the BTMB formed in high-temperature environments, and the depletion of Sr, P, and Ti indicates characteristics of continental arc granite, which may be related to the collision of the Bayan Hara and East Kunlun Blocks along the BTMB in Late Hercynian–Early Triassic.

Generally, the geochemical–element ratios of island arc basalts and partially depleted mid-ocean ridge basalts are Nb/La < l, Hf/Ta > 5, La/Ta > 15, and Ti/Y < 350, while those of intraplate basalts, transitional mid-ocean ridge basalts, and enriched mid-ocean ridge basalts are considerably different (Condie 1989; Fitton 2007; Niu 2016). The diabase dikes in the BTMB have Nb/La ratios of 0.25–0.33, Hf/Ta ratios of 3.25–8.19, La/Ta ratios of 30.36–74.63, and Ti/Y ratios of 174.85–346.53. This suggests that the formation settings of these diabase dikes are unrelated to the lithotectonic settings of intraplate basalt, transitional mid-oceanic ridge basalt, and enriched mid-oceanic ridge basalt, as is the case for island arc basalt and depleted mid-ocean ridge basalt. The element ratios of island arc basalts are Th/Yb > 0.1, Th/Nb > 0.07, Nb/La < 0.8, and Hf/Th < 8, whereas those of depleted mid-ocean ridge basalts are considerably different (Condie 1989; Fitton 2007; Niu 2016). The diabase dikes in the BTMB have Th/Yb ratios of 6.37–8.38, Th/Nb ratios of 0.95–1.52, Nb/La ratios of 0.25–0.33, and Hf/Th ratios of 0.11–0.54, which are clearly of island arc nature. The diorite dike in the BTMB has Nb/La ratios of 1.02–2.22, Hf/Ta ratios of 0.97–2.20, La/Ta ratios of 5.80–13.44, Ti/Y ratios of 96.18–405.17, Th/Yb ratios of 4.95–7.70, Th/Nb ratios of 0.23–0.64, and Hf/Th ratios of 0.11–0.76, mostly similar or close to the ratios of the diabase dikes.

Therefore, it is after the Bayan Hara Block subduction or collision with the East Kunlun Block in Late Hercynian–Early Triassic that mantle melt was enriched during crustal relaxation, was emplaced up along tensile faults, and was contaminated by crustal materials, forming the Late Triassic dikes.

Tectonic significance

Since the Buqingshan–A'nyemaqen ocean subduction, the EKOB developed several calcium metaluminous potassium basic character arc magmatic rocks during the subduction stage of 260–240 Ma (Guo et al. 1998; Yang et al. 2005; Mo et al. 2007; Chen et al. 2013a, b, c, 2017a, 2018a, b, c; Liu et al. 2014; Chen et al. 2016; Hu et al. 2016; Hu et al. 2017; Zhang et al. 2017; Li et al. 2018a; Fig. 8a). Intrusive rocks in the East Kunlun area that are associated with the 240 to 225 Ma collision between the Bayan Hara and East Kunlun Blocks are rare. This stage of intrusive rocks have the syn-collision granite characteristics (Zhang et al. 2012; Xia et al. 2014; Xiong et al. 2015; Chen et al. 2018b; Fig. 8b). After the Late Triassic, post-collision granitoids are represented by the stitching Gerizhuoto diorite pluton in the BTMB, which suggests that by then, the Buqingshan–A'nyemaqen Ocean had

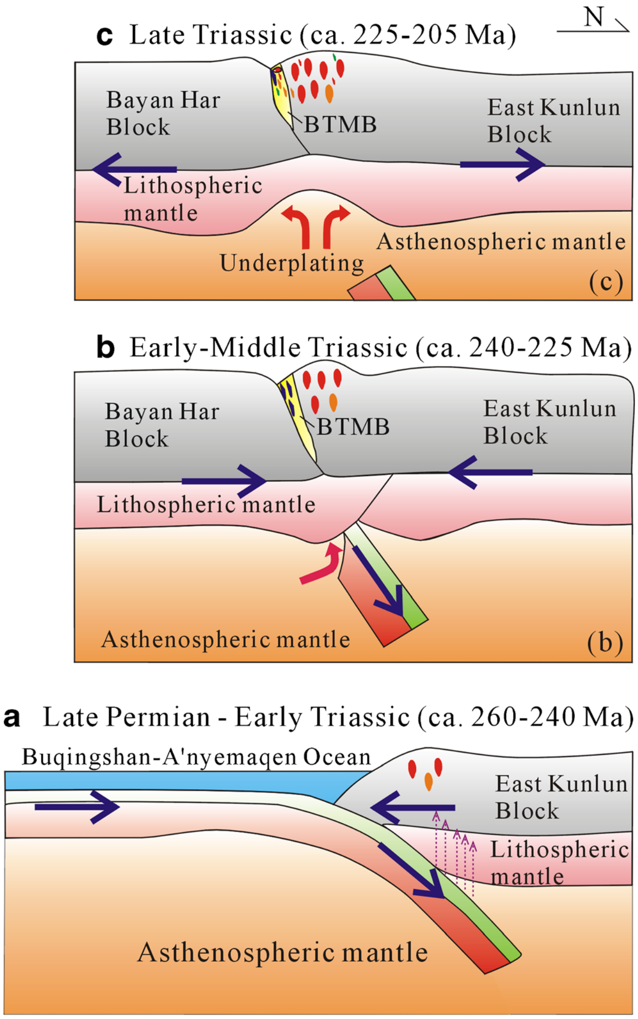

Fig. 8 Schematic diagrams illustrating the tectonic and magmatic evolution of in the BTMB, southern margin of the EKOB **a** subduction stage (260–240 Ma). **b** Collision stage (240–225 Ma). **c** Post-collision stage (225–205)

already been closed (225.8 ± 1.5 Ma, Li et al. 2013c; Fig. 8c). In the southern part of the EKOB, north of the BTMB, the angular unconformities between the Babaoshan Formation (T_3b) and the overlain Middle Triassic Naocangjiangou Formation (T_2n) and between continental volcanic rocks and the underlying strata of the Upper Triassic Erashan Formation (T_3e) in the northern part of the East Kunlun area mark the end of continental collision between the Bayan Hara and East Kunlun Blocks (Liu et al. 2011a; Li et al. 2012).

Comparison of dikes in the BTMB with the 226 Ma Binggou mafic dike swarm of the EKOB (Liu et al. 2017) reveals that at least since the Late Triassic, the EKOB had shifted from compressional to extensional environments (Liu et al. 2017), and intermediate–basic dikes in the BTMB formed later than the various abovementioned intrusive rocks. These results show that at ~ 225 Ma, the BTMB and the adjacent area had entered a post-orogenic extension stage (Fig. 8c), as also indicated by the development of the stitching pluton and mafic dike swarm. This implies that the intermediate–basic dikes in BTMB are the product of the post-orogenic intracontinental extension tectonic setting, suggesting that in 225–205 Ma, the BTMB was at the post-orogenic stress–relaxation stage of Bayan Hara Block subduction–collision with the East Kunlun Block (Fig. 8c). Decompression melting of the post-collision stage lifted the thermal interface, thereby inducing the melting of the mantle wedge and the formation of the abovementioned dikes.

Conclusions

Our comprehensive geochronological and geochemical study of the intermediate–basic dikes in the BTMB (along the southern margin of the EKOB, Tibetan Plateau, China) provides the following conclusions:

(1) Geochemical analyses show that the dikes have the characteristics of arc magmatic suites. REEs have low concentrations and incline to the right with weak negative Eu anomalies. The diorite dike magma was formed at high temperature (~ 777 °C) by partial melting of mantle material and possibly was contaminated by crustal material when ascending.

(2) The zircon U–Pb age of the diorite dike is 205 ± 1 Ma (MSWD = 0.88), which shows that the intrusion formed in the Late Triassic (Rhaetian) and thus also represents the latest tectonic magmatism in the BTMB.

(3) The intermediate–basic dikes in the BTMB are the products of enriched mantle upwelled and emplaced in the crustal relaxation period after the subduction–collision of the Bayan Har and East Kunlun Blocks during the Late Hercynian–Early Triassic.

Acknowledgments We would like to thank the editor, Prof. Abdullah M. Alamri and four anonymous reviewers for the helpful comments that helped clarify our results. We are indebted to Dr. Paul D. Bons, professor of Eberhard Karls University Tübingen, for his academic guidance support and advice. We wish to acknowledge Saping Ding, Junfeng Guo, Jianyun Feng, Yu Sun, Yafeng Zhang, Gang Zhang, and others for their help during the fieldwork, and Zhou Hui at the Beijing SHRIMP Center for assistance with taking CL images; Dr. Xiaoming Liu and Dr. Chunrong Diwu, at the Northwest University, State Key Laboratory of Continental Dynamics, for assistance with LA–ICP–MS dating; and He Li at the Institute of Geology and Geophysics, State Key Laboratory of Lithosphere Evolution, for assistance with conducting XRF and trace element analyses. The authors would like to thank Enago (www.enago.cn) for the English language review.

Funding information This study was supported financially by the National Nature Sciences Foundation of China (Grant Nos. 41872233, 41872235, 41802234, 41602229, 41472191, 41502191, 41172186, and 40972136), the Commonweal Geological Survey, The Aluminum Corporation of China and the Land–Resources Department of Qinghai Province (Grant No. 200801), China Geological Survey (Grant Nos. 12120114041201, and DD2016007901), China Scholarship Council

(Grant No. 201806565026), China Postdoctoral Science Foundation (Grant No. 2016M592726), and the Fundamental Research Funds for the Central Universities of China (Grant Nos. 300103183081, 300104282717, 300102279204, and 201810710233).

References

Andersen T (2002) Correction of common lead in U–Pb analyses that do not report ^{204}Pb. Chem Geol 192(1–2):59–79

Barth MG, McDonough WF, Rudnick RL (2000) Tracking the budget of Nb and Ta in the continental crust. Chem Geol 165(3–4):197–213

Bea F (2012) The sources of energy for crustal melting and the geochemistry of heat–producing elements. Lithos 153:278–291

Belousova EA, Griffin WL, O'Reilly SY, Fisher N (2002) Igneous zircon: trace element composition as an indicator of source rock type. Contrib Mineral Petrol 143(5):602–622

Bian QT, Zheng XS (1992) Structure characteristics and tectonic evolution of Kekexili area in Qinghai. In: Xu GZ, Chang CF (eds) Continental lithosphere structure and resources. Ocean Press, Beijing, pp 19–32

Bian QT, Li DH, Pospelov I, Yin LM, Li HS, Zhao DS, Chang CF, Luo XQ, Gao SL, Astrakhahtsev O, Chamov N (2004) Age, geochemistry and tectonic setting of Buqingshan Ophiolites, North Qinghai–Tibet Plateau, China. J Asian Earth Sci 23(4):577–596

Bian QT, Luo XQ, Li DH, Zhao DS, Chen HH, Xu GZ, Chang CF, Gao YL (2001a) Geochemistry and formation environment of the Buqingshan ophiolite complex, Qinghai Province, China. Acta Geol Sin 75(1):45–55

Bian QT, Luo XQ, Chen HH, Zhao DS, Li DH (1999a) Zircon U–Pb age of granodiorite–tonalite in the A'nyemaqen ophiolitic belt and its tectonic significance. Sci Geol Sin 34(4):420–426

Bian QT, Luo XQ, Li HS, Chen HH, Zhao DS, Li DH (1999b) Discovery of early Paleozoic and early Carboniferous–early Permian ophiolites in the A'nymaqen, Qinghai province, China. Sci Geol Sin 34(4): 523–524

Bian QT, Pospelov II, Li HM, Chang CF, Li JL (2007) Discovery of the end–early Paleozoic adakite in the Buqingshan area, Qinghai province, and its tectonic implications. Acta Petrol Sin 23(5):925–934

Bian QT, Yin LM, Sun SF, Luo XQ, Pospelov II, Astrakhahtsev O, Chamov N (2001b) Discovery of Ordovician suspected sources in the Buqushan ophiolite melange of East Kunlun. Chin Sci Bull 46(2):167–171

Bian QT, Yin LM, Sun SF, LuoXQ PII, Astrakhahtsev O, Chamov N (2001c) Discovery of Ordovician acri–tarchs in Buqingshan ophiolite complex, east Kunlun mountains and its significance. Chin Sci Bull 46(4):341–345

Burchfiel BC, Molnar P, Zhao ZY, Liang KY, Wang SJ, Huang MM, John S (1989) Geology of the Ulugh Muztagh area, northern Tibet. Earth Planet Sci Lett 94(1–2):57–70

Chai YC, Feng BG, Yang JS (1984) On the geological feature and genesis of the granitic zone in the Dong–Xidatan area of Middle-Eastern Kunlun Mountains. In: Contribution to the geology of the Qinghai–Xizang (Tibet) plateau (15). Geological Society of China, Beijing

Chen FK, Hegner E, Todt W (2000b) Zircon ages, Nd isotopic and chemical compositions of orthogneisses from the Black Forest, Germany: evidence for a Cambrian magmatic arc. Int J Earth Sci (Geol Rundsch) 88:791–802

Chen FK, Siebel W, Satir M, Terzioglu MN, Saka K (2002b) Geochronology of the Karadere basement (NW Turkey) and implications for the geological evolution of the Istanbul zone. Int J Earth Sci (Geol Rundsch) 91:469–481

Chen G, Pei XZ, Li ZC, Li RB, Chen YX, Liu CJ, Chen GC, Wang XB, Sang JZ, Yang S, Deng WB (2016) Zircon U–Pb geochronology, geochemical characteristics and geological significance of Chaohuolutaolegai granodiorite in Balong area, East Kunlun Mountains. Geol Bull China 35(12):1990–2005

Chen GC, Pei XZ, Li RB, Li ZC, Liu CJ, Chen YX, Pei L, Li XB (2018b) Age and lithogenesis of Keri syenogranite from eastern part of east Kunlun Orogenic Belt: constraint on the Middle Triassic tectonic evolution of East Kunlun. Acta Petrol Sin 34(3):567–585

Chen GC, Pei XZ, Li RB, Li ZC, Liu CJ, Chen YX, Pei L, Wang M, Li XB (2017b) Paleo-Tethyan oceanic crust subduction in the eastern section of the East Kunlun Orogenic Belt: geochronology and petrogenesis of the Qushi'ang granodiorite. Acta Geol Sin–Engl 91(2): 565–580

Chen GC, Pei XZ, Li RB, Li ZC, Liu CJ, Chen YX, Pei L, Zhang YM, Wang M, Li XB, Zhang Y (2017a) Age and petrogenesis of Jialuhe basic–intermediate pluton in Xiangjia'nanshan granite batholith in the eastern part of East Kunlun Orogenic Belt, and its geological significance. Geotecton Metallog 41(6):1097–1115

Chen GC, Pei XZ, Li RB, Li ZC, Pei L, Liu CJ, Chen YX, Li XB (2018a) Triassic magma mixing and mingling at the eastern section of eastern Kunlun: a case study from Xiangjiananshan granitic batholith. Acta Petrol Sin 34(8):2441–2480

Chen GC, Pei XZ, Li RB, Li ZC, Pei L, Liu CJ, Chen YX, Wang M, Zhang Y, Li XB (2018c) Magma mixing in Halagatu granitic batholith from eastern part of the East Kunlun Orogenic Belt: constraints from lithology and mineralogy. Earth Sci 43(9):3200–3217

Chen GC, Pei XZ, Li RB, Li ZC, Pei L, Liu ZQ, Chen YX, Liu CJ (2013b) Late Triassic magma mixing in the East Kunlun orogenic belt: a case study of Helegang Xilikete granodiorites. Geol China 40(4):1044–1065

Chen GC, Pei XZ, Li RB, Li ZC, Pei L, Liu ZQ, Chen YX, Liu CJ, Gao JM, Wei FH (2013a) Zircon U–Pb geochronology, geochemical characteristics and geological significance of Cocoe A'Long quartz diorites body from the Hongshuichuan area in East Kunlun. Acta Geol Sin 87(2):178–196

Chen GC, Pei XZ, Li RB, Li ZC, Pei L, Liu ZQ, Chen YX, Liu CJ, Gao JM, Wei FH (2013c) Geochronology and genesis of the Helegang Xilikete granitic plutons from the southern margin of the eastern East Kunlun Orogenic Belt and their tectonic significance. Acta Geol Sin 87(10):1525–1541

Chen L, Sun Y, Liu XM, Pei XZ (2000a) Geochemistry of Derni ophiolite and its tectonic significance. Acta Petrol Sin 16(1):106–110

Chen L, Sun Y, Pei XZ (1999) Derni ophiolite: northernmost Tethyan lithosphere relics in Tibet Plateau. J Northwest Univ (Nat Sci) 29(2): 51–54

Chen L, Sun Y, Pei XZ, Feng T, Zhang GW (2004) Comparison of eastern paleo–Tethyan ophiolites and its geodynamic significance: evidence from Dur'ngoi ophiolite. Sci China Ser D Earth Sci 47(4):378–384

Chen W, Guo YR, Cui B, Arnaud N, Zhang JX, Zhang Y (2002a) Research on the isotopic ages of the deformations and metamorphisms of the Xidatan rock series, East Kunlun Mountains. Geol Rev 48(Supp):103–109

China University of Geosciences (Wuhan) Geological Survey (2000) 1 : 250000 Donggeicuolahu regional geological survey report, unpublished

Claesson V, Vetrin T, Bayanova HD (2000) U–Pb zircon ages from a Devonian carbonatite dyke. Kola peninsula, Russia: a record of geological evolution from the Archaean to the Palaeozoic. Lithos 51: 95–108

Condie KC (1989) Geochemical changes in basalts and and sites across the Archaean–Proterozoic boundary: identification and significance. Lithos 23:1–18

Deng WB, Pei XZ, Liu CJ, Li ZC, Li RB, Chen YX, Chen GC, Yang S, Chen G, Sang JZ, Wang XB (2016) LA–ICP–MS zircon U–Pb dating of the Chahantaolegai syenogranites in Xiangride area of East Kunlun and its geological significance. Geol Bull China 35(5):687–699

Ding QF, Jiang SY, Sun FY (2014) Zircon U–Pb geochronology, geochemical and Sr–Nd–Hf isotopic compositions of the Triassic granite and diorite dikes from the Wulonggou mining area in the eastern Kunlun Orogen, NW China: Petrogenesis and tectonic implications. Lithos 205:266–283

Dong YP, He DF, Sun SS, Liu XM, Zhou XH, Zhang FF, Yang Z, Cheng B, Zhao GC, Li JH (2018) Subduction and accretionary tectonics of the east Kunlun orogen, western segment of the Central China orogenic system. Earth-Sci Rev 186:231–261

England PC, Thompson A (1986) Some thermal and tectonic models for crustal melting in continental collision zones. In: Coward MP, Ries AC (eds) Collision tectonics. Geol Soc Lond Spec Pub 19:83–94

Fitton JG (2007) The OIB paradox. In: Foulger GR, Jurdy DM (eds) Plates, plumes, and planetary processes. Spec Pap–Geol Soc Am, vol 430, pp 387–412

Gao XY, Zheng YF (2011) On the Zr–in–rutile and Ti–in–zircon geotherm meters. Acta Petrol Sin 27(2):418–632

Green TH (1995) Significance of Nb/Ta as an indicator of geochemical processes in the crust–mantle system. Chem Geol 120(3–4):347–359

Green TH, Pearson NJ (1986) Ti-rich accessory phase saturation in hydrous maficfelsic compositions at high P, T. Chem Geol 54:185–201

Green TH, Pearson NJ (1987) An experimental study of Nb and Ta partitioning between Ti–rich minerals and silicate liquids at high pressure and temperature. Geochim Cosmochim Acta 51(1):55–62

Griffin WL, Pearson NJ, Belousova E, Jackson SE, Achterbergh EV, O'Reilly SY, Shee SR (2000) The Hf isotope composition of cratonic mantle: LAM–MC–ICP MS analysis of zircon megacrysts in kimberlites. Geochim Cosmochim Acta 64(1):133–147

Guo AL, Zhang GW, Sun YG, Cheng SY, Yao AP (2007) Geochemistry and spatial distribution of late–Paleozoic mafic volcanic rocks in the surrounding areas of the Gonghe basin: implications for Majixueshan triplejunction and east Paleotethyan archipelagic ocean. Sci China Ser D Earth Sci 50(Supp II):292–304

Guo ZF, Deng JF, Xu ZQ, Mo XX, Luo ZH (1998) Late Palaeozoic-Mesozoic intracontinental orogenic process and intermediate-acidic igneous rocks from the eastern Kunlun Mountains of northwestern China. Geoscience 12(3):344–352

Han QJ, Shao JA, Zhou R (2000) Petrology, geochemistry and petrogenesis of Early Mesozoic diorites in Har–qin area, inner–Mongolia. Acta Petrol Sin 16(3):385–391

Hanchar JM, Westrenen WV (2007) Rare earth element behavior in zircon_melt systems. Elements 3(1):37–42

Harris NBW, Xu RH, Lewis CL, Hawkesworth CJ, Zhang YQ (1988) Isotope geochemistry of the 1985 Tibet Geotraverse, Lhasa to Golmud. Philos Trans R Soc Lond 327(1594):263–285

Harrison TM, Watson EB (1984) The behavior of apatite during crustal anatexisequilibrium and kinetic considerations. Geochim Cosmochim Acta 48:1467–1477

Hartmann LA (2001) SHRIMP U–Pb isotopic analyses of zircon as applied to metallogeny and crustal evolution. Gondwana Res 4(2): 227–230

Hasterok D, Webb J (2017) On the radiogenic heat production of igneous rocks. Geosci Front 8:919–940

Hoskin PWO (2005) Trace element composition of hydrothermal zircon and the alteration of Hadean zircon from the Jack Hills, Australia. Geochim Cosmochim Acta 69(3):637–648

Hoskin PWO, Black LP (2000) Metamorphic zircon formation by solid_state recrystallization of protolith igneous zircon. J Metamorph Geol 18:423–439

Hoskin PWO, Ireland TR (2000) Rare earth element chemistry of zircon and its use as a provenance indicator. Geology 28(7):627–630

Hoskin PWO, Schaltegger U (2003) The composition of zircon and igneous and metamorphic petrogenesis. Rev Mineral Geochem 53(1): 27–62

Hu CG, Pei XZ, Li RB, Chen YX, Liu CJ, Li ZC, Zhang Y, Yan QZ, Wang X, Peng SZ (2017) Zircon U–Pb ages and geological significance of metamorphic basic intrusive rocks in the acite area of East Kunlun. Northwest Geol 50(1):182–197

Hu Y, Niu YL, Li JY, Ye L, Kong JJ, Chen S, Zhang Y, Zhang GR (2016) Petrogenesis and tectonic significance of the late Triassic mafic dikes and felsic volcanic rocks in the East Kunlun Orogenic Belt, northern Tibet Plateau. Lithos 245:205–222

Jiang CF, Wang ZQ, Li JY (2000) Open and close structure of central orogenic belt. Geol Publ House, Beijing

Jiang CF, Yang JS, Feng BG, Zhu ZZ, Zhao M, Chai YC (1992) Opening closing tectonics of Kunlun mountains. Geol Publ House, Beijing

Kieffer B, Arndt N, Lapierre H, Bastien F, Bosch D, Pecher A, Yirgu G, Ayalew D, Weise D, Jerram DA, Keller F, Meugniot C (2004) Flood and shield basalts from Ethiopia: magmas from the African Superswell. J Petrol 45(4):793–834

Li RB, Pei XZ, Li ZC, Chen YX, Liu CJ, Pei L, Xu T, Liu ZQ, Wei B (2015a) Geological and geochemical features of Delisitannan basalts and their Petrogenesis in Buqingshan tectonic mélange belt, Southern Margin of East Kunlun Orogen. Earth Sci (J China Univ Geosci) 40(7):1148–1162

Li RB, Pei XZ, Li ZC, Liu ZQ, Chen GC, Chen YX, Wei FH, Gao JM, Liu CJ, Pei L (2012) Geological characteristics of Late Palaeozoic–Mesozoic unconformities and their response to some significant tectonic events in eastern part of eastern Kunlun. Earth Sci Front 19(5):244–254

Li RB, Pei XZ, Li ZC, Pei L, Chen GC, Chen YX, Liu CJ (2017a) Late Cambrian SSZ–type ophiolites in Acite Zone, East Kunlun Orogen of northern Tibet Plateau: insights from zircon U–Pb isotopes and geochemistry of oceanic crust rocks. Acta Geol Sin–Engl 91(S1): 66–67

Li RB, Pei XZ, Li ZC, Pei L, Chen GC, Liu CJ, Chen YX, Liu ZQ (2014a) Geochemical characteristics of Gerizhuotuo OIB and its tectonic significance in Buqingshan tectonic. Earth Sci Front 21(1):183–195

Li RB, Pei XZ, Li ZC, Pei L, Chen GC, Wei B, Chen YX, Liu CJ, Wang M (2018b) Cambrian (~510 Ma) ophiolites of the East Kunlun orogen, China: a case study from the Acite ophiolitic tectonic mélange. Int Geol Rev 60(16):2063–2083

Li RB, Pei XZ, Li ZC, Pei L, Liu CJ, Chen YX, Chen GC, Liu ZQ, Yang J (2015b) Geochemistry and zircon U–Pb geochronology of granitic rocks in the Buqingshan tectonic mélange belt, northern Tibet Plateau, China and its implications for Prototethyan evolution. J Asian Earth Sci 105:374–389

Li RB, Pei XZ, Li ZC, Sun Y, Feng JY, Pei L, Chen GC, Liu CJ, Chen YX (2013b) Geochemical features, age and tectonic significance of the Kekekete mafic–ultramafic rocks, east Kunlun orogen. China Acta Geol Sin–Engl 87(5):1319–1333

Li RB, Pei XZ, Li ZC, Sun Y, Pei L, Chen GC, Chen YX, Liu CJ, Wei FH (2013a) Regional tectonic transformation in east Kunlun orogenic belt in early Paleozoic: constraints from the geochronology and geochemistry of Helegananaren alkali–feldspar granite. Acta Geol Sin–Engl 87(2):333–345

Li RB, Pei XZ, Pei L, Li ZC, Chen GC, Chen YX, Liu CJ, Wang M (2018a) The Early Triassic Andean–type Halagatu granitoids pluton in the East Kunlun orogen, northern Tibet Plateau: response to the northward subduction of the paleo–Tethys Ocean. Gondwana Res 62:212–226

Li RB, Pei XZ, Wei B, Li ZC, Pei L, Chen YX, Liu CJ, Chen GC, Wang M, Feng K (2019) Constraints of late Cambrian mafic rocks from the Qushi'ang ophiolite on a back–arc system in a continental margin, East Kunlun Orogen, Western China. J Asian Earth Sci 169:117–129

Li WY, Li SG, Guo AL, Sun YG, Zhang GW (2007) Zircon SHRIMP U–Pb ages and trace element geochemistry of the Tamachian gabbro and the Daritic diorite in the east Kunlun Tectonic Belt of Qinghai

Province–comparison of the Late Neoproterozoic–Early Ordovician Ages in “Qi–Chai–Kun” Island Ocean South Boundary Constraints. Sci China Ser D Earth Sci 50(Suppl.II):331–338

Li ZC, Li RB, Pei L, Chen YX, Liu CJ, Pei XZ, Liu ZQ, Chen GC, Li XB (2018c) Magmatic response to the proto–Tethyan Ocean subduction in east section of East Kunlun: evidence from zircon U–Pb dating of the late Sinian Dundeshaerguole hornblende monzonite. Earth Sci 43(12):4536–4550

Li ZC, Pei XZ, Li RB, Pei L, Liu CJ, Chen YX, Liu ZQ, Chen GC, Xu T, Yang J, Wei B (2014b) Geochronology, geochemistry and tectonic setting of the Bairiqiete granodiorite intrusion (rock mass) from the Buqingshan tectonic mélange belt in the southern margin of East Kunlun. Acta Geol Sin–Engl 88(2):584–597

Li ZC, Pei XZ, Li RB, Pei L, Liu CJ, Chen YX, Zhang YM, Wang M, Xu T (2017b) Early Ordovician Island–arc type Manite granodiorites pluton (rock mass) from the Buqingshan tectonic mélange belt in the southern margin of East Kunlun: constraints on closure of the proto–Tethys Ocean. Geol J 52:510–528

Li ZC, Pei XZ, Liu ZQ, Li RB, Pei L, Chen GC, Liu CJ, Chen YX, Gao JM, Wei FH, Wu SK, Wang YC, Yang J (2013c) Geochronology and geochemistry of the gerizhuotuo diorites from the Buqingshan tectonic mélange belt in the southern margin of East Kunlun and their geologic implications. Acta Geol Sin 87(8):1090–1103

Liu B, Ma CQ, Huang J, Wang LX, Zhao SQ, Yan R, Sun Y, Xiong FH (2017) Petrogenesis and tectonic implications of Upper Triassic appinite dykes in the East Kunlun orogenic belt, northern Tibetan Plateau. Lithos 284(285):766–778

Liu B, Ma CQ, Zhang JY, Xiong FH, Huang J, Jiang HA (2014) ^{40}Ar-^{39}Ar age and geochemistry of subduction-related mafic dikes in northern Tibet, China: petrogenesis and tectonic implications. Int Geol Rev 56(1):57–73

Liu CD, Mo XX, Luo ZH, Yu XH, Chen HW, Li SW, Zhao X (2004) Mixing events between the crust- and mantle-derived magmas in Eastern Kunlun: evidence from zircon SHRIMP II chronology. Chin Sci Bull 49(8):828–834

Liu ZQ, Pei XZ, Li RB, Li ZC, Chen GC, Chen YX, Gao JM, Liu CJ, Wei FH, Wang XL, Zhang G (2011c) Early Paleozoic intermediate–acid magmatic activity in Bairiqiete area along the Buqingshan tectonic mélange belt on the southern margin of east Kunlun: constraints from zircon U–Pb dating and geochemistry. Geol China 38(5): 1150–1167

Liu ZQ, Pei XZ, Li RB, Li ZC, Chen YX, Gao JM, Liu CJ, Wang XL, Wei FH, Zhang G, Yang ZZ (2011b) Geological characteristics of the tectonic mélange belt of Buqingshan area in the southern margin of east Kunlun and its tectonic implications. Geol Bull China 30(8): 1182–1195

Liu ZQ, Pei XZ, Li RB, Li ZC, Zhang XF, Liu ZG, Chen GC, Chen YX, Ding SP, Guo JF (2011a) LA–ICP–MS zircon U–Pb geochronology of the two suites of ophiolites at the Buqingshan area of the A’nyemaqen orogenic belt in the southern margin of east Kunlun and its tectonic implication. Acta Geol Sin 85(2):185–194

Ludwig KR (2003) Isoplot 3.0–a geochronological toolkit for Microsoft Excel. Berkeley Geochronology Center Spec Pub 4:1–70

McDonough WF, Sun SS (1995) The composition of the Earth. Chem Geol 120:223–253

Mo XX, Luo ZH, Deng JF, Yu XH, Liu CD, Chen HW, Yuan WM, Liu YH (2007) Granitoids and crustal growth in the East–Kunlun orogenic belt. Geol J China Univ 13(3):403–414

Mo XX, Pan GT (2006) From the Tethys to the formation of the Qinghai–Tibet Plateau: constrained by tectono–magmatic events. Earth Sci Front 13(6):43–50

Molnar P, Burchfiel BC, Zhao ZY, Liang KY, Wang SJ, Huang MM (1987) Geologic evolution of northern Tibet: results of an expedition to Ulugh Muztagh. Science 235:299–305

Niu YL (2016) The meaning of global ocean ridge basalt major element compositions. J Petrol 57(11–12):2081–2104

Pan GT, Wang LQ, Li RS, Yuan SH, Ji WH, Yin FG, Zhang WP, Wang BD (2012) Tectonic evolution of the Qinghai–Tibet Plateau. J Asian Earth Sci 53:3–14

Patino–Douce AE, Johnston AD (1991) Phase equilibria and melt productivity in the pelitic system: implications for the origin of peraluminous granitoids and aluminous granulites. Contrib Mineral Petrol 107(2):202–218

Pei L, Li RB, Pei XZ, Liu JL, Li ZC, Liu CJ, Chen YX, Liu ZQ, Chen GC, Hu N, Gao F (2017) Sediment source analysis for the Maérzheng formation sandstone in Gerizhuotuo area, southern margin of East Kunlun region: evidence for detrital zircon U–Pb geochronology. Acta Geol Sin 91(6):1326–1344

Pei XZ (2001) Geological evolution and dynamics of the Miaulue–A’nyemaqen tectonic zone, central China. Northwest University, Xi’an

Pei XZ, Hu N, Liu CJ, Li RB, Li ZC, Chen YX, Pei L, Liu ZQ, Chen GC, Yang J (2015) Detrital composition, geochemical characteristics and provenance analysis for the Maerzheng Formation sandstone in Gerizhuotuo area, southern margin of East Kunlun Region. Geol Rev 61(2):307–323

Pei XZ, Li RB, Li ZC, Liu CJ, Chen YX, Pei L, Liu ZQ, Chen GC, Li XB, Wang M (2018) Composition feature and formation process of Buqingshan composite accretionary mélange belt in southern margin of East Kunlun orogen. Earth Sci 43(12):4498–4520

Rickwood PC (1989) Boundary lines within petrologic diagrams which use oxides of major and minor elements. Lithos 22(4):247–263

Rollinson HR (1993) Using geochemical data: evaluation, presentation, interpretation. Longman Scientific and Technical, New York

Rubatto D (2002) Zircon trace element geochemistry: partitioning with garnet and the link between U–Pb ages and metamorphism. Chem Geol 184:123–138

Saunders AD, Storey M, Kent RW, Norry MJ (1992) Consequences of plume–lithosphere interactions. In: Storey BC, Alabaster T, Pankhurst RJ (eds) Magmatism and the causes of continental breakup. Geo Soc Lond Spec Pub 68:41–60

Siebel W, Blaha U, Chen FK, Johann R (2005) Geochronology and geochemistry of a dyke–host rock association and implications for the formation of the Bavarian Pfahl shear zone, Bohemian Massif. Int J Earth Sci (Geol Rundsch) 94(1):8–23

Sun SS, McDonough WF (1989) Chemical and isotopic systematics of ocean basins: implications for mantle composition and processes. In: Saunders AD, Norry MJ (eds) Magmatism of the ocean basins. Geol Soc Lond Spec Pub 42:325–345

Sun Y, Pei XZ, Ding SP, Li RB, Feng JY, Zhang YF, Li ZC, Chen YX, Zhang XF, Chen GC (2009) Halagatu magma mixing granite in the East Kunlun Mountains: evidence from zircon U–Pb dating. Acta Geol Sin 83(7):1000–1010

Tapia–Fernandez HJ, Armstrong–Altrin JS, Selvaraj K (2017) Geochemistry and U–Pb geochronology of detrital zircons in the Brujas beach sands, Campeche, southwestern Gulf of Mexico, Mexico. J S Am Earth Sci 76:346–361

Thompson AB, Connolly JAD (1995) Melting of the continental crust: some thermal and petrological constraints on anatexis in continental collision zones and other tectonic settings. J Geophys Res Solid Earth 100(B8):15565–15579

Vanderhaeghe O (2009) Migmatites, granites and orogeny: flow modes of partially–molten rocks and magmas associated with melt/solid segregation in orogenic belts. Tectonophysics 477:119–134

Vavra G, Schmid R, Gebauer D (1999) Internal morphology, habit and U–Th–Pb microanalysis of amphibolite–to–granulite facies zircons: geochronology of the Ivrea Zone (Southern Alps). Contrib Mineral Petrol 134(4):380–404

Wang GC, Zhang KX, Liang B, Zhang Z (1997b) Texture and tectonic slices of the eastern Kunlun orogenic belt. Earth Sci (J China Univ Geosci) 22(4):352–356

Wang GC, Zhang TP, Liang B, Chen NS, Zhu YH, Zhu J, Bai YS (1999) Composite Ophiolitic Melange zone in central part of eastern section of eastern Kunlun orogenic zone and geological significance of “Fault Belt in central part of eastern section of eastern Kunlun orogenic zone”. Earth Sci (J China Univ Geosci) 24(2):129–138

Wang X, Chen J, Griffin WL, O’reilly SY, Huang PY, Li X (2011) Two stages of zircon crystallization in the Jingshan monzogranite, Bengbu uplift: implications for the syn–collisional granites of the Dabie–Sulu UHP orogenic belt and the climax of movement on the Tan–Lu fault. Lithos 122(3–4):201–213

Wang YB, Huang JC, Luo MS, Tian J, Bai YS (1997a) Paleo–ocean evolution of the southern eastern Kunlun Orogenic Belt during Hercy–Early Indosinian. Earth Sci (J China Univ Geosci) 22(4): 369–372

Watson EB, Wark DA, Thomas JB (2006) Crystallization thermometers for zircon and rutile. Contrib Mineral Petrol 151:413–433

Wu FY, Zhang YB, Yang JH, Xie LW, Yang YH (2008) Zircon U–Pb and Hf isotopic constraints on the Early Archean crustal evolution in Anshan of the North China Craton. Precambrian Res 167(3–4): 339–362

Wu YB, Zheng YF (2004) Genesis of zircon and its constraints on interpretation of U–Pb age. Chin Sci Bull 49(15):1554–1569

Xia R, Wang CS, Deng J, Carranza EJM, Li WL, Qing M (2014) Crustal thickening prior to 220Ma in the East Kunlun Orogenic Belt: insights form the Late Triassic granitoids in the Xiao-Nuomuhong pluton. J Asian Earth Sci 93:193–210

Xiong FH, Ma CQ, Wu L, Jiang HA, Liu B (2015) Geochemistry, zircon U–Pb ages and Sr–Nd–Hf isotopes of an Ordovician Appinitic pluton in the East Kunlun orogen: new evidence for proto–Tethyan subduction. J Asian Earth Sci 111:681–697

Xu ZQ, Li HB, Yang JS (2006d) An orogenic plateau: the orogenic collage and orogenic types of the Qinghai–Tibet Plateau. Earth Sci Front 13(4):1–17

Xu ZQ, Li HB, Yang JS, Chen W (2001) A large transpression zone at the south margin of the East Kunlun Mountains and oblique subduction. Acta Geol Sin 75(2):156–164

Xu ZQ, Yang JS, Chen FY (1996) A’nyemaqen suture and subduction–collision dynamics. In: Zhang Q (ed) Study on ophiolites and dynamics. Geol Publ House, Beijing

Xu ZQ, Yang JS, Li HB, Yao JX (2006a) The early Palaeozoic terrene framework and the formation of the high–pressure (HP) and ultra–high pressure (UHP) metamorphic belts at the central orogenic belt (COB). Acta Geol Sin 80(12):13–26

Xu ZQ, Yang JS, Li HB, Yao JX (2006c) The Early Palaeozoic terrene framework and the formation of the high–pressure(HP)and ultra–high pressure(UHP) metamorphic belts at the Central Orogenic Belt (COB). Acta Geol Sin 80(12):1793–1806

Xu ZQ, Yang JS, Li HB, Zhang JX, Zeng LS, Jiang M (2006b) The Qinghai–Tibet plateau and continental dynamics: a review on terrain tectonics, collisional orogenesis, and processes and mechanisms for the rise of the plateau. Geol China 33(2):221–238

Xu ZQ, Yang JS, Li WC, Li HQ, Cai ZH, Yan Z, Ma CQ (2013) Paleo–Tethys system and accretionary orogen in the Tibet Plateau. Acta Petrol Sin 29(6):1847–1860

Yang JS, Wang XB, Shi RD, Xu ZQ, Wu CL (2004) The Dur’ngoi ophiolite in east Kunlun, northern Qinghai–Tibet Plateau: a fragment of paleo–Tethyan oceanic crust. Geol China 31(3):225–238

Yang JS, Xu ZQ, Li HB, Shi RD (2005) The paleo–Tethyan volcanism and plate tectonic regime in the A’nyemaqen region of East Kunlun, northern Tibet Plateau. Acta Petrol Et Mineral 24(5):369–380

Yang S, Pei XZ, Li RB, Liu CJ, Chen YX, Li ZC, Wang XB, Sang JZ, Chen G, Deng WB (2016) Provenance analysis and structural implications of Gequ Formation at the Buqingshan area in the eastern segment of the East Kunlun region. Geol Bull China 35(5):674–686

Yin HF, Zhang KX (1997) Characteristics of the eastern Kunlun orogenic belt. Earth Sci. J China Univ Geosci 22(4):339–342

Yuan HL, Gao S, Liu XM, Li HM, Günther D, Wu FY (2004) Accurate U–Pb age and trace element determinations of zircon by laser ablation–inductively coupled plasma mass spectrometry. Geostand Geoanal Res 28(3):353–370

Yuan HL, Wu FY, Gao S, Liu XM, Xu P, Sun DY (2003) Determination of U–Pb age and rare earth element concentrations of zircons from Cenozoic intrusions in northeastern China by laser ablation ICP–MS. Chin Sci Bull 48(22):2411–2421

Zhang CL, Diwu CR, Kroner A, Sun Y, Luo JL, Li QL, Gou LL, Lin HB, Wei XS, Zhao J (2015) Archean–Paleoproterozoic crustal evolution of the Ordos block in the North China craton: constraints from zircon U–Pb geochronology and Hf isotopes for gneissic granitoids of the basement. Precambrian Res 267:121–136

Zhang GW, Dong YP, Lai SC, Guo AL, Meng QR, Liu SF, Cheng SY, Yao AP, Zhang ZQ, Pei XZ, Li SZ (2003) Mianle tectonic zone and Mianle suture zone on southern margin of Qinling–Dabie orogenic belt. Sci China Ser D Earth Sci 47(4):300–316

Zhang KX, Huang JC, Luo MS, Zhang TP, Bai YS (1999) Sedimentary geochemical features of A’nimaqing mélange zone in eastern Kunlun mountains. Earth Sci (J China Univ Geosci) 24(2):111–115

Zhang JY, Ma CQ, Xiong FH, Liu B (2012) Petrogenesis and tectonic significance of the Late Permian-Middle Triassic calc-alkaline granites in the Balong region, eastern Kunlun Orogen, China. Geol Mag 149(5):892–908

Zhang Y, Pei XZ, Li RB, Liu CJ, Chen YX, Li ZC, Wang X, Hu CG, Yan QZ, Peng SZ (2017) Zircon U–Pb geochronology, geochemistry of the Alasimu gabbro in eastern section of East Kunlun Mountains and the closing time of paleo–ocean basin. Geol China 44(3):526–540

Zhao ZH (2010) Trace element geochemistry of accessory minerals and its applications in petrogenesis and metallogenesis. Earth Sci Front 17(1):268–285

Zhu YH, Zhang KX, Pan YM, Chen NS, Wang GC, Hou GJ (1999) Determination of different ophiolitic belts in eastern Kunlun orogenic zone and their tectonic significance. Earth Sci (J China Univ Geosci) 24(2):134–138